Precambrian Research 255 (2014) 748–755

Contents lists available at ScienceDirect

Precambrian Research

journal homepage: www.elsevier.com/locate/precamres

Detrital zircon constraint on the timing of amalgamation between Alxa and Ordos, with exploration implications for Jinchuan-type Ni–Cu ore deposit in China

Qingyan Tang[a], Chusi Li[b,c], Mingjie Zhang[a,*], Edward M. Ripley[c], Qili Wang[a]

[a] School of Earth Sciences and Gansu Key Laboratory of Mineral Resources in Western China, Lanzhou University, Lanzhou 730000, China
[b] State Key Laboratory of Ore Deposit Geochemistry, Institute of Geochemistry, Chinese Academy of Sciences, Guiyang 550002, China
[c] Department of Geological Sciences, Indiana University, Bloomington, IN 47405, USA

ARTICLE INFO

Article history:
Received 4 October 2013
Received in revised form 10 August 2014
Accepted 26 August 2014
Available online 3 September 2014

Keywords:
Zircon U–Pb–Lu–Hf isotopes
Trace elements
Magmatic sulfide deposit
Jinchuan
Alxa
North China Craton

ABSTRACT

The Jinchuan Ni–Cu deposit, which is the largest single magmatic sulfide ore deposit in the world, is hosted by a mafic-ultramafic intrusion in the Alxa block, northwestern China. The timing of amalgamation between the Alxa block and the adjacent Ordos block, which is important for Precambrian reconstruction of North China Craton and the search for another Jinchuan-type ore deposit, is contentious. The age distribution patterns of detrital zircon crystals with Precambrian ages from the Devonian and older sedimentary rocks of the Alxa and Ordos blocks are similar. This supports the traditional view that the Alxa and Ordos blocks were amalgamated in the Paleoproterozoic along the 1.95 Ga Khondalite Belt, long before the emplacement of the ~830 Ma Jinchuan intrusion. The U–Pb–Lu–Hf isotope data of comagmatic zircon crystals from the Jinchuan intrusion, together with its whole-rock Sm–Nd isotopes and trace element compositions given previously by other researchers, indicate that the Jinchuan ore-bearing intrusion is the product of continental rift-related basaltic magmatism which took place during the early stage of Rodinia breakup. Based on these observations, we conclude that in addition to the Alxa block, the adjacent regions in the North China Craton such as the Ordos basin, the Khondalite belt and the Yinshan terrane are most promising for new discoveries of Jinchuan-type Ni–Cu ore deposits.

1. Introduction

The Alxa (or Alashan) block is located in northwestern China (Fig. 1). Many researchers believe that the Alxa block and the adjacent Ordos block of the North China Craton were amalgamated in the Paleoproterozoic along ~1.95 Ga Khondalite Belt between them (e.g., Zhao et al., 2001, 2005; Lu et al., 2008; Zhao and Cawood, 2012; Zhang J. et al., 2013; Peng et al., 2014). However, different opinions also exist. Li et al. (2005) proposed that the Alxa block is an exotic continental block derived from South China after the breakup of Rodinia. This view is based on the assumption that the ~830 Ma Jinchuan Ni–Cu sulfide ore-bearing mafic-ultramafic intrusion in the Alxa block and the contemporaneous mafic-ultramafic intrusions in West Yangtze (Fig. 1) are the products of the so-called South China mantle superplume, which is proposed to have been active during Rodinia breakup (Li et al., 1999, 2002, 2003b). Based on the apparent differences in the timing and nature of magmatism and metamorphism from Neoarchean to Paleoproterozoic times deduced from rocks in the Alxa block and the nearby Yinshan terrane in the North China Craton (Fig. 1), Dan et al. (2012a) contended that the Alxa block was separated from the North China Craton in the Paleoproterozoic. Based on apparent different detrital zircon age distribution patterns between the Middle-Early Devonian sandstones of the Alxa block and the Ordovician and older sedimentary rocks of the Ordos block, Yuan and Yang (2014) concluded that these two blocks were separated before Late Devonian. A resolution to the above debate is important not only for the Precambrian reconstruction of North China Craton but also for the search for another Jinchuan-type Ni–Cu ore deposit in China. In this paper, we use detrital zircon age data for the Devonian and older sedimentary rocks of the Alxa and Ordos blocks, and the comagmatic zircon U–Pb–Lu–Hf isotopes and whole-rock geochemical data for the Jinchuan intrusion to address these important issues.

2. Tectonic division

The North China, South China and Tarim are three major Precambrian continental blocks that were assembled to form China

* Corresponding author.
E-mail address: mjzhang@lzu.edu.cn (M. Zhang).

http://dx.doi.org/10.1016/j.precamres.2014.08.015
0301-9268/

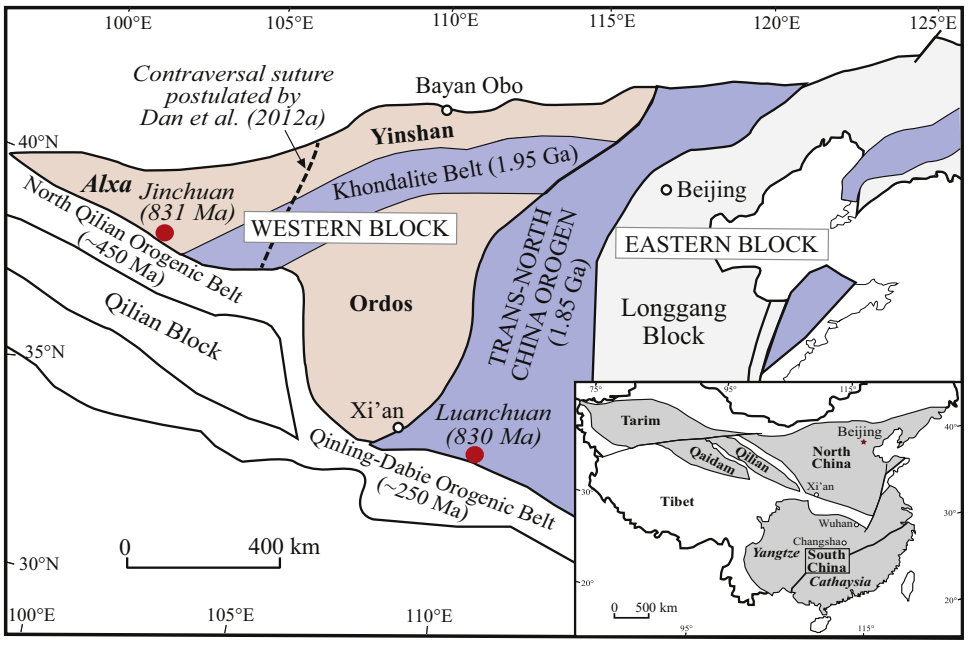

Fig. 1. Simplified maps showing the tectonic units of China (modified from Zhao and Cawood, 2012).

during Phanerozoic times (Fig. 1). The South China Block comprises the Yangtze Craton in the north and the Cathaysia Block in the south (Fig. 1), separated by the Sibao (Li et al., 2002) or Jiangnan (Zhao and Cawood, 1999; Charvet, 2013) Proterozoic Orogenic Belt. The Yangtze Craton consists of Archean–Paleoproterozoic crystalline basement surrounded by late Mesoproterozoic to early Neoproterozoic folded belts, which are locally unconformably overlain by weakly metamorphosed Neoproterozoic strata and unmetamorphosed Sinian cover (Zhao and Cawood, 2012). The Cathaysia block is composed predominantly of Neoproterozoic metamorphic rocks, with minor Paleoproterozoic and Mesoproterozoic lithologies. Archean basement is poorly exposed (Zhao and Cawood, 2012; Charvet, 2013) and largely inferred from detrital zircons from Neoproterozoic sedimentary rocks (Yu et al., 2010).

The North China Craton is bounded by the late Paleozoic Central Asian Orogenic Belt to the north (Xiao et al., 2003), by the Permian-Triassic Qinling-Dabie Orogenic Belt to the southeast (Hacker et al., 1998; Li et al., 2003a), and by the ~450 Ma North Qilian Orogenic Belt to the southwest (Song et al., 2013). The North China Craton consists of Archean to Paleoproterozoic metamorphic basement overlain by Mesoproterozoic to Cenozoic unmetamorphosed cover. It is divided into the Eastern and Western Blocks (Fig. 1), separated by the Trans-North China Orogenic Belt with a final collision age of ~1.85 Ga (Zhao et al., 2008; Zhao and Cawood, 2012). The Western Block is further divided into the Ordos Block in the south and the Yinshan Block in the north, separated by the Khondalite Belt with a final collision age of ~1.95 Ga (Zhao et al., 2010; Dan et al., 2012b). The Khondalite Belt is also referred to as the Fengzhen Belt (Peng et al., 2010; Zhai and Santosh, 2011) or the Inner Mongolian Suture Zone (Santosh, 2010).

Li et al. (2005) suggested that the Alxa block was derived from South China after Rodinia breakup. Dan et al. (2012a) and Yuan and Yang (2014) believe that the Alxa block (Fig. 1) was separated from the rest of the North China Craton in the Paleoproterozoic. In contrast, Zhai and Santosh (2011) believe that the Alxa block was part of the North China Craton as early as 2.5 Ga. Zhang J. et al. (2013) believe that the Alxa block is the extension of the Khondalite Belt of the North China Craton.

3. Geological background

The Jinchuan ore-bearing mafic-ultramafic intrusion occurs in the eastern part of the Longshoushan terrane at the southern rim of the Alxa block (Figs. 1 and 2a). To the south the Longshoushan terrane is bounded by the North Qilian Orogenic Belt which formed by the collision between the Alxa block and the North Qilian block at ~450 Ma (Song et al., 2013). Regional metamorphism of greenschist facies related to the collision event has affected the Longshoushan terrane including the Jinchuan intrusion. The Jinchuan intrusion intruded the Proterozoic Baijiazuizi Formation which comprises marbles, gneisses, and granitic migmatites (Fig. 2b). Abundant Paleozoic granites occur farther to the south (Fig. 2a). Li et al. (2005) reported a U–Pb SHRIMP zircon age of 827 ± 8 Ma for the Jinchuan intrusion. Zhang et al. (2010) reported a precise ID-TIMS zircon U–Pb age of 831.8 ± 0.6 Ma obtained on thermally annealed and chemically etched zircon grains from the intrusion.

The current surface exposure of the Jinchuan intrusion measures ~6500 m long and ~500 m wide (Fig. 2b). The overall strike of the intrusion is northwest. The vertical downward extension of the intrusion exceeds 1100 m in its central part. The Jinchuan intrusion is composed almost entirely of peridotites. Rare gabbros occur in the margins of the intrusions in a few places. Mineralization occurs predominantly as disseminated to net-textured sulfides within the intrusion. The Jinchuan deposit contains >500 million metric tons of sulfide ores with grades of 1.1 wt.% Ni and 0.7 wt.% Cu, and is the largest single magmatic Ni–Cu sulfide ore deposit in the world (Li and Ripley, 2011; Zhang M. et al., 2013).

4. Samples and analytical methods

4.1. Samples

A large lherzolite sample (JC11-04, ~10 kg) from the Jinchuan intrusion (Fig. 2b) was used for whole-rock chemistry, zircon U–Pb age determination and zircon Lu–Hf isotope study. This sample is composed of 65 vol.% olivine, 17 vol.% clinopyroxene, 13 vol.% orthopyroxene, and minor amphibole. Clinopyroxene

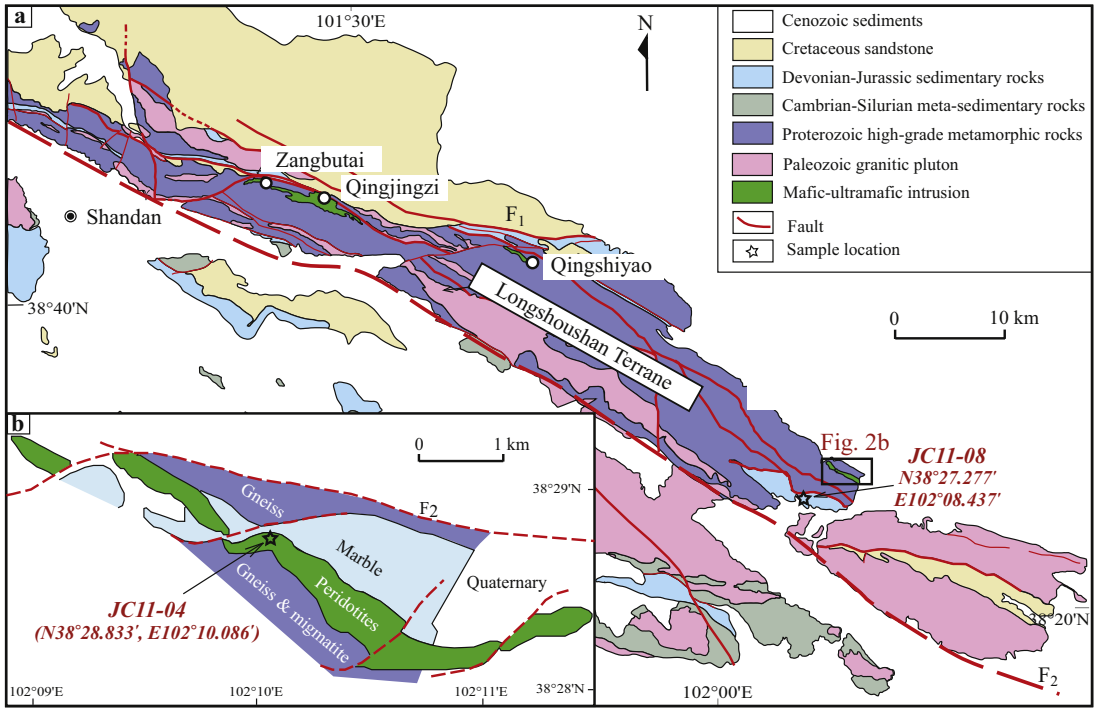

Fig. 2. Simplified geologic maps of the Longshoushan terrane (a) and Jinchuan mafic-ultramafic intrusion (b), after Li and Ripley (2011).

commonly occurs as large crystals enclosing small olivine crystals. Pyroxenes, hornblende and phlogopite occur in the interstitial spaces.

A large early-Devonian sandstone sample (JC11-08, ~5 kg) from the Longshoushan terrane (Fig. 2a) was used for detrital zircon U–Pb dating and Lu–Hf isotopic study. This sample is fine-grained. It contains ~55 vol.% quartz, ~15 vol.% feldspars and ~35 vol.% Fe–Mg silicate minerals plus heavy minerals. Micro-carbonate veins are abundant in the sample. Zircon crystals in both samples were separated using conventional techniques including magnetic separation, heavy liquids and hand-picking.

4.2. Analytical methods

Whole-rock major and trace element compositions were determined by XRF and by inductively coupled plasma mass spectrometry (ICP-MS), respectively, at Chang'an University, Xi'an, China. Rock powders were fused to form glass disks for XRF analysis, and acid-digested in steel-jacketed Teflon "bombs" to form solutions for ICP-MS analysis. The analytical uncertainties are between 5% and 15% relative, depending on the concentrations of elements in the samples.

Zircon U–Pb isotope analysis was performed using a SHRIMP-II machine and Neptune multi-collector ICP-MS equipped with a New Wave UP 213 laser-ablation sampling system in the Chinese Academy of Geological Sciences, Beijing. The analytical procedures and operation conditions for SHRIMP and LA-MC-ICP-MS are given in Williams (1998) and Hou et al. (2009), respectively. Plotting and age calculations are from Isoplot/Ex 3.00 Ludwig (2003).

Zircon Lu–Hf isotopes were determined in situ using LA-MC-ICP-MS in the MRL Key Laboratory of Metallogeny and Mineral Assessment, Institute of Mineral Resources, Chinese Academy of Geological Sciences, Beijing, following the procedures given in Wu et al. (2006). The laser beam size was about 40–50 μm in diameter. The GJ1 zircon standard was used as a reference.

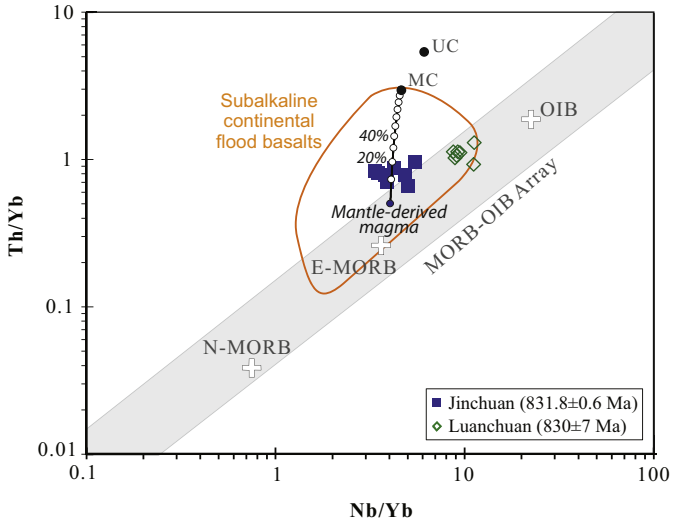

Fig. 3. Plot of Nb/Yb versus Th/Yb in whole rocks. The sources of data: Jinchuan (Li et al., 2005; Zhang et al., 2010; this study); Luanchuan (Wang et al., 2011); continental flood basalts (GeoRoc online database). The mantle array is from Pearce (2008). The average composition of the middle continental crust is from Rudnick and Gao (2003).

5. Results

5.1. Geochemical fingerprinting for the Jinchuan intrusion

The chemical composition of the Jinchuan lherzolite is given in Supplementary Table A1 (available online). A comparison of whole-rock Th/Yb and Nb/Yb ratios between the Jinchuan intrusion and subalkaline continental flood basalts worldwide is illustrated in Fig. 3. It is well known that mafic-ultramafic intrusive rocks are commonly crystal cumulates plus variable amounts of "trapped liquids". The effect of crystal accumulation on the trace element ratios of these rocks needs to be adjusted before they can be

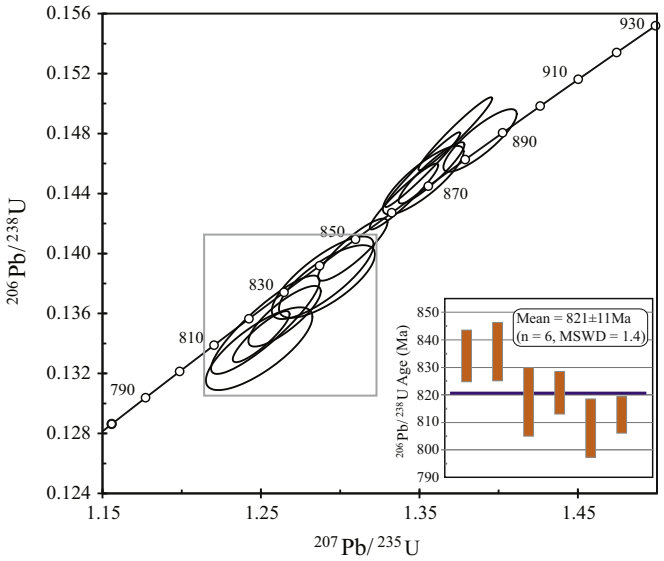

Fig. 4. Concordia diagram with a weighted mean ^{206}Pb/^{238}U age for the six youngest, comagmatic zircons from the Jinchuan lherzolite.

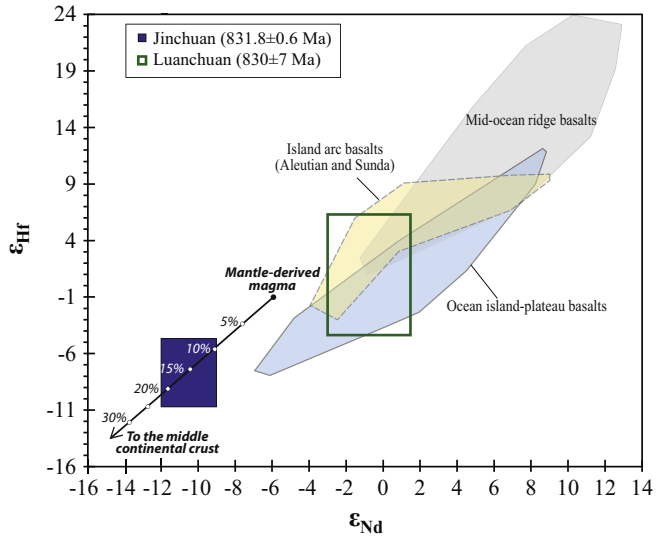

Fig. 5. Plot of zircon ε_{Hf} (t) versus whole-rock ε_{Nd} (t) for the Jinchuan mafic-ultramafic intrusion. Data sources: Jinchuan (Li et al., 2005; Zhang et al., 2010; this study), Luanchuan (Wang et al., 2011), Aleutian and Sunda arcs (Handley et al., 2011; Yogodzinski et al., 2010), mid-ocean ridge basalts and ocean island-plateau basalts (Salters et al., 2011).

compared to flood basalts. Olivine, pyroxenes and plagioclase are commonly the most important cumulus minerals in the intrusive rocks. Among these cumulus minerals clinopyroxene may have the largest effect on the distribution of Th, Nb and Yb in these rocks because the solid–liquid partition coefficients of these incompatible trace elements for clinopyroxene are higher than those for olivine and plagioclase (Wood and Blundy, 2003). Li et al. (2013) showed that the trace element ratios of arc cumulates containing Yb > 0.5 ppm closely matched those of "trapped liquids" in the samples. This value is adapted as a cut-off value for sample selection in our comparison. The selected samples for the Jinchuan mafic-ultramafic intrusion and the contemporaneous Luanchuan mafic intrusion which occurs in the western part of the North China Craton (Fig. 1) all plot within the field of global continental flood basalts. The Jinchuan samples plot slightly above the E-MORB and toward the average continental middle crust (Fig. 3). Simple mixing calculation using an assumed mantle-derived magma containing 9.6 ppm Nb, 1.2 ppm Th and 2.4 ppm Yb, which are similar to those in the E-MORB, and the average continental middle crust composition given by Rudnick and Gao (2003) indicates that the Jinchuan parental magma may have experienced up to 20% crustal contamination (Fig. 3). In contrast, no significant crustal contamination is required to explain the trace element compositions of the contemporaneous Luanchuan mafic intrusion.

The U–Pb isotopic compositions of zircons from the Jinchuan lherzolite determined by LA-MC-ICP-MS are given in Supplementary Table A2 (available online). Fig. 4 is a concordia diagram for all zircons from the Jinchuan lherzolite. The six youngest, comagmatic zircons give a weighted mean ^{206}Pb/^{238}U age of 821 ± 11 Ma, which is within the range of previously reported, more precise zircon U–Pb ages for the Jinchuan intrusion by Li et al. (2005) and Zhang et al. (2010).

The Lu–Hf isotopes of comagmatic zircons from the Jinchuan lherzolite are listed in Table 1. The calculated ε_{Hf} (t) values of these zircons vary from −5 to −11. The comagmatic zircon ε_{Hf} and whole-rock ε_{Nd} values for the Jinchuan mafic-ultramafic intrusion are significantly lower than the values for plume-related basalts in oceanic settings (ocean islands and oceanic plateaus) (Fig. 5). In contrast, the comagmatic zircon ε_{Hf} and whole-rock ε_{Nd} values for the contemporaneous Luanchuan mafic intrusion are within the ranges of the plume-related basalts in oceanic settings. Back calculation by allowing a maximum of 22% contamination with the middle continental crust for the Jinchuan parental magma indicates that the source mantle of the Jinchuan intrusion is isotopically more depleted than that of the coeval Luanchuan mafic intrusion (Fig. 5).

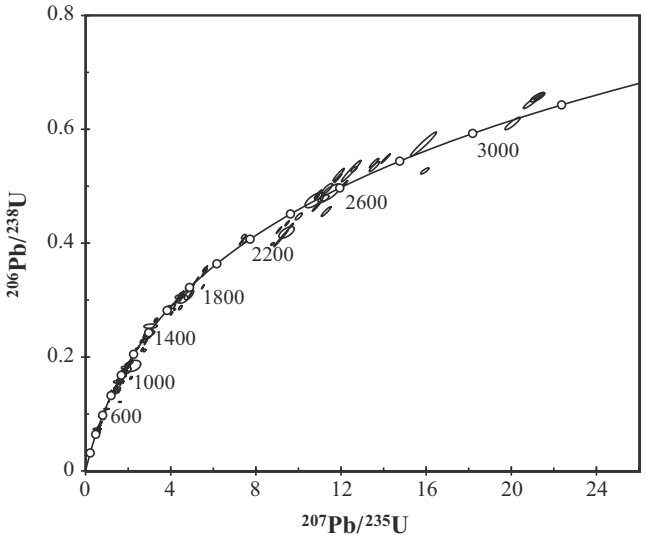

Fig. 6. Concordia diagram for detrital zircons from early-Devonian sandstone in Longshoushan, Alxa, North China Block.

5.2. Detrital zircon data

The chemical composition of an early-Devonian sandstone sample from the Longshoushan terrane, Alxa block is given in Supplementary Table A1 (available online). The U–Pb–Lu–Hf isotopic compositions of detrital zircon crystals from this sample, determined by LA-MC-ICP-MS and SHRIMP, are given in Table 1 and Supplementary Table A2 and Table A3 (available online). A couple of duplicate analyses show that the U-Pb isotopes determined using the different analytical techniques show <3% variation. The data listed in the tables and shown in the concordia plot (Fig. 6) are the 217 analyses with degrees of concordance >90%. The other 28 analyses with degrees of concordance <90% are discarded. The

Table 1
Lu–Hf isotopes of zircons from the Jinchuan intrusion and a sandstone sample from Longshoushan, Alxa.

Analysis	Age (Ma)	$^{176}Yb/^{177}Hf$	2σ	$^{176}Lu/^{177}Hf$	2σ	$^{176}Hf/^{177}Hf$	2σ	$(^{176}Hf/^{177}Hf)_i$	$\varepsilon_{Hf}(t)$	T_{DM} (Ma)
Lherzolite, Jinchuan intrusion (831 Ma)										
JC11-04-08	821	0.034784	0.000681	0.000640	0.000016	0.281967	0.000024	0.281957	−10.7	1792
JC11-04-14	836	0.038637	0.000104	0.000775	0.000004	0.282130	0.000024	0.282118	−4.7	1573
JC11-04-20	813	0.039210	0.000601	0.000698	0.000001	0.282128	0.000020	0.282117	−5.2	1573
JC11-04-22	818	0.033315	0.000118	0.000620	0.000005	0.282082	0.000020	0.282073	−6.7	1632
JC11-04-23	834	0.034030	0.000444	0.000620	0.000004	0.282080	0.000019	0.282070	−6.4	1635
JC11-04-24	809	0.038732	0.000085	0.000681	0.000003	0.282093	0.000018	0.282083	−6.6	1620
Early-Devonian sandstone from Longshoushan, Alxa										
JC11-08-3.1	1128	0.018497	0.000341	0.000706	0.000008	0.282342	0.000018	0.282327	9.1	1276
JC11-08-4.1	937	0.022572	0.000080	0.000570	0.000001	0.282331	0.000023	0.282321	4.6	1287
JC11-08-5.1	1746	0.023959	0.000476	0.000711	0.000013	0.281750	0.000022	0.281727	1.8	2092
JC11-08-07	924	0.032388	0.000965	0.001013	0.000028	0.282045	0.000020	0.282027	−6.1	1702
JC11-08-10	834	0.033960	0.000603	0.001372	0.000019	0.281703	0.000026	0.281682	−20.3	2195
JC11-08-14	971	0.050768	0.000737	0.001653	0.000035	0.282216	0.000025	0.282186	0.6	1488
JC11-08-18.1	2455	0.071037	0.000726	0.001709	0.000011	0.281290	0.000026	0.281210	−0.4	2791
JC11-08-19	834	0.024425	0.000784	0.000719	0.000010	0.282063	0.000020	0.282052	−7.2	1663
JC11-08-21	1435	0.043162	0.000520	0.001050	0.000012	0.281644	0.000021	0.281615	−9.2	2258
JC11-08-23	834	0.034956	0.000328	0.000825	0.000004	0.282089	0.000029	0.282076	−6.4	1631
JC11-08-26.1	947	0.021333	0.000200	0.000505	0.000001	0.281846	0.000027	0.281837	−12.3	1951
JC11-08-28	2531	0.025636	0.000049	0.000731	0.000018	0.281244	0.000019	0.281208	1.3	2782
JC11-08-34.1	1748	0.031983	0.000359	0.001030	0.000010	0.281578	0.000018	0.281544	−4.7	2346
JC11-08-36.1	950	0.022476	0.000412	0.000542	0.000007	0.282120	0.000025	0.282110	−2.6	1577
JC11-08-84	890	0.048262	0.000479	0.001513	0.000022	0.282321	0.000026	0.282296	2.7	1334
JC11-08-89	2514	0.019245	0.000049	0.000552	0.000001	0.281000	0.000021	0.280973	−7.4	3097
JC11-08-96	844	0.014931	0.000661	0.000466	0.000023	0.281812	0.000028	0.281804	−15.8	1996
JC11-08-100	984	0.002399	0.000017	0.000047	0.000000	0.282012	0.000025	0.282012	−5.3	1703
JC11-08-118	739	0.024437	0.000183	0.000873	0.000007	0.282417	0.000037	0.282405	3.2	1177
JC11-08-139	1526	0.048936	0.000140	0.001210	0.000003	0.282131	0.000028	0.282096	9.9	1589
JC11-08-141	3084	0.030801	0.001086	0.000778	0.000028	0.280883	0.000028	0.280836	0.9	3272
JC11-08-157	846	0.033614	0.000185	0.000835	0.000002	0.281897	0.000026	0.281883	−12.9	1898
JC11-08-161	1439	0.061237	0.001062	0.001462	0.000020	0.282085	0.000027	0.282046	6.1	1664
JC11-08-163	876	0.066119	0.000272	0.002154	0.000005	0.281878	0.000025	0.281843	−13.7	1992
JC11-08-170	1277	0.043705	0.000185	0.001025	0.000002	0.281922	0.000030	0.281897	−2.8	1872
JC11-08-180	2553	0.016393	0.000179	0.000434	0.000002	0.281005	0.000021	0.280984	−6.1	3080
JC11-08-182	2552	0.017151	0.000141	0.000453	0.000001	0.281268	0.000026	0.281246	3.1	2730
JC11-08-188	787	0.042885	0.000219	0.001206	0.000009	0.281442	0.000024	0.281424	−30.5	2545
JC11-08-191	870	0.062754	0.000156	0.001861	0.000006	0.282386	0.000023	0.282356	4.4	1253
JC11-08-207	803	0.058756	0.000548	0.002146	0.000035	0.281934	0.000027	0.281902	−13.2	1912
JC11-08-210	3122	0.014206	0.000055	0.000353	0.000002	0.280865	0.000027	0.280843	2.1	3261

Zircon crystallization ages younger and older than 1000 Ma are calculated from $^{206}Pb/^{238}U$ and $^{207}Pb/^{206}Pb$, respectively.
ε_{Hf} at the age of zircon crystallization was calculated using CHUR values of Blichert-Toft and Albarède (1997) and ^{176}Lu decay constant of Scherer et al. (2001).
T_{DM} was calculated from present-day depleted mantle values of $^{176}Hf/^{177}Hf = 0.28325$ and $(^{176}Lu/^{177}Hf)_{DM} = 0.0384$ (Griffin et al., 2000).

zircon ages are calculated using the $^{206}Pb/^{238}U$ ratios for those younger than 1000 Ma and the $^{207}Pb/^{206}Pb$ ratios for those older than 1000 Ma.

Fig. 7a illustrates the age distribution of detrital zircon crystals from an early-Devonian sandstone sample from the Longshoushan terrane used in this study. Fig. 7b is the age distribution spectrum of detrital zircon crystals from the Devonian and older sedimentary rocks of the Alxa block based on all available analyses to date. In this plot, 153 analyses are for detrital zircon crystals from the Taerling Dam, the eastern part of the Alxa block (Zhang et al., 2012), 361 analyses are for detrital zircon crystals from western Langshan, the northeastern part of the Alxa block (Hu et al., 2014), and 1154 analyses are for detrital zircon crystals from Longshoushan, the southern part of the Alxa block (Tung et al., 2007; Gong et al., 2011, 2013; Yuan and Yang, 2014; this study). Fig. 7c is the age distribution spectrum of detrital zircon crystals from the Ordovician and older sedimentary rocks of the Ordos block (Darby and Gehrels, 2006; Zhang et al., 2011).

A comparison between Fig. 7b and c reveals that the Alxa and Ordos blocks have similar and different detrital zircon age spectra before and after the Cambrian Period, respectively. The detrital zircons with Precambrian ages from both blocks are all characterized by three prominent age peaks at 0.9–1.0 Ga, 1.8–2.1 Ga and 2.5 Ga. In more detail, the size and shape of the 1.8–2.1 Ga detrital zircon age peak are slightly different between these two blocks. However, this may have resulted from insufficient data for the Ordos block.

As shown in Fig. 7b and c, the prominent detrital zircon age peak at ~450 Ma is present in the samples from the Alxa block but absent in the samples from the Ordos block. A close examination of the data reveals that the ~450 Ma detrital zircon age peak for the Alxa block is produced by the Devonian sandstone samples from the Longshoushan terrane which is bounded by the ~450 Ma North Qilian orogenic belt to the south (Fig. 1).

6. Discussion

6.1. Timing of amalgamation between Alxa and Ordos blocks

As shown in Fig. 2, abundant Ordovician granitoids occur across the boundary between the Longshoushan terrane and the North Qilian orogenic belt to the south. After sufficient uplifting and weathering, these granitoids could have supplied significant amounts of detrital zircon crystals to the Devonian sandstones in the Longshoushan terrane, producing the prominent detrital zircon age peak at ~450 Ma (Fig. 7b).

There are several reasons that may explain the absence of this detrital zircon age peak in the samples from the Ordos block. Firstly, the youngest deposition age of the Ordos samples used in the comparison is Ordovician, not much different from the ages of the granitoids in the North Qilian orogenic belt. As a result, there was not enough time for the Ordovician granitoids in the North Qilian orogenic belt to be uplifted and weathered, and thereby to

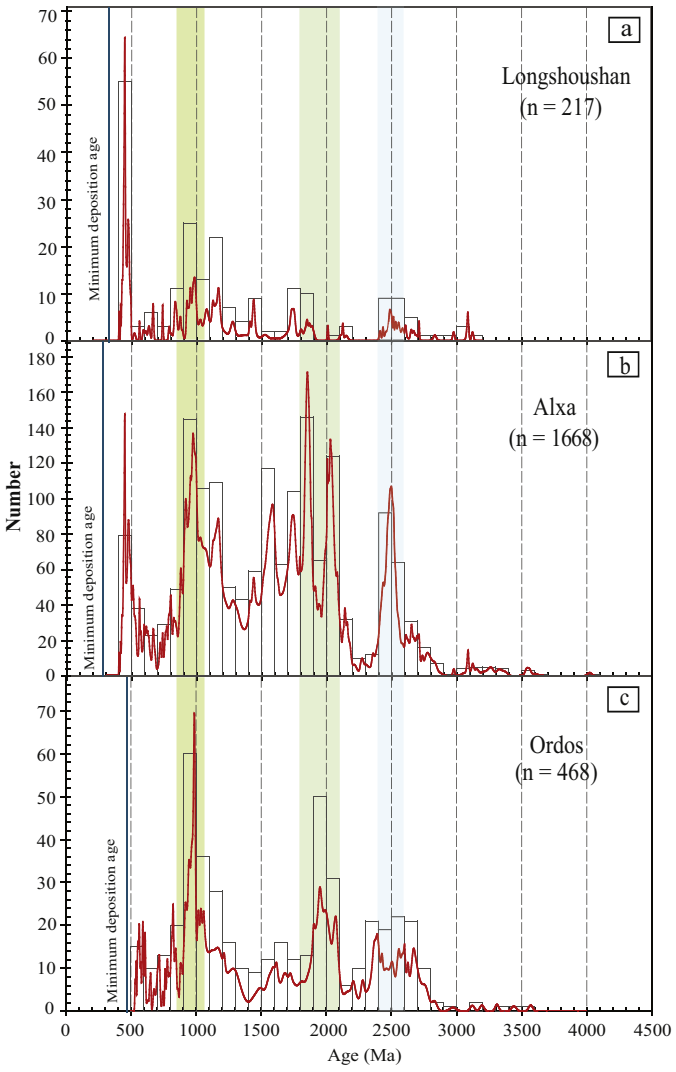

Fig. 7. Age spectra of detrital zircon crystals from early-Devonian and older sedimentary rocks in the Alxa block and from pre-Devonian sedimentary rocks in the Ordos block. Data sources: Longshoushan (this study), Alxa (Tung et al., 2007; Gong et al., 2011, 2013; Zhang et al., 2012; Hu et al., 2014; Yuan and Yang, 2014; this study), Ordos (Darby and Gehrels, 2006; Zhang et al., 2011).

supply significant amounts of detrital zircon crystals to the Ordovician sediments in the Ordos basin. Secondly, the Ordos basin was possibly blocked from the North Qilian orogenic belt in the Paleozoic by the N-S trending Helan Mt. (or Helanshan), the southernmost part of the Khondalite belt (Fig. 1). Thirdly, the Paleozoic orogenic belt containing syncollisional granitoids, which occurs along the southern margin of the Ordos block, i.e., the E Qilian-W Qinling segment, formed after ~400 Ma (e.g., Hacker et al., 1998), much younger than the deposition ages of the sedimentary rock samples from the Ordos block used in the comparison.

The similarity in the age spectra of detrital zircon crystals with Precambrian ages between the Alxa and Ordos blocks described above is consistent with the traditional view that these two blocks were amalgamated in the Paleoproterozoic, possibly along the 1.95 Ga Khondalite Belt between them (Fig. 1) (e.g., Zhao et al., 2001, 2005; Lu et al., 2008; Zhao and Cawood, 2012; Zhang J. et al., 2013; Peng et al., 2014). Yuan and Yang (2014) used the existence of two prominent age peaks, one at 488 Ma and the other at ~1.0 Ga, for the detrital zircon crystals from the Middle-Late Devonian sandstones of the Longshoushan terrane in the Alxa block, and the absence of these age peaks for the detrital zircon crystals from the Ordovician and older sedimentary rocks of the Ordos block to argue against the assembly of these two blocks in the Paleoproterozoic. However, this argument is difficult to substantiate. Firstly, the ~1.0 Ga detrital zircon age peak is in fact also present in the pre-Devonian sedimentary rocks of the Ordos block (see Fig. 7c). The reason that they failed to recognize this is because the data for the Ordos block from Zhang et al. (2011) were not included in their comparison. Secondly, as discussed above, there is alternative and perhaps better explanation for the absence of the ~450 Ma detrital zircon age peak in the pre-Devonian sedimentary rock samples from the Ordos block.

In addition to similar age distribution spectra of detrital zircon crystals from the pre-Devonian sedimentary rocks between the Alxa and Ordos blocks, the age distribution spectra of comagmatic zircon crystals from igneous rocks between these two blocks are also similar (see data compiled by Hu et al., 2014). As shown in Hu et al. (2014), the Precambrian age peaks of both detrital and comagmatic zircon crystals from these two blocks generally match each other. This is significant because the most important ultimate source of detrital zircon crystals is granitoids that contain far more zircon crystals than mafic-ultramafic rocks. Since most granitoids were produced during large-scale crustal growth, the similar zircon age peaks between the Alxa and Ordos blocks indicate that these two blocks have similar histories of lithosphere evolution in the Precambrian. This supports the interpretation that these two blocks were together prior to the emplacement of the ~830 Ma Jinchuan Ni–Cu sulfide ore-bearing intrusion.

6.2. *Exploration targeting of Jinchuan-type ore deposit*

Li et al. (2005) suggested that the Longshoushan terrane in the Alxa block was part of the South China block prior to the emplacement of the ~830 Ma Jinchuan mafic-ultramafic intrusion and that this intrusion was produced by a hypothetical mantle superplume which also produced the contemporaneous mafic-ultramafic intrusions in the Guibei region, West Yangtze, such as the Baotan, Sanfang and Yuanbaoshan intrusions (Li et al., 1999, 2003b). If this model is correct, the search for another Jinchuan-type Ni–Cu ore deposit should be focused on South China, more specifically on the Guibei region. Given the evidence described above, we do not agree with this model. We believe that the Alxa block was part of the North China Block prior to the emplacement of the Jinchuan intrusion. According to this model, the search for another Jinchuntype ore deposit should be focused on the North China Block. More specifically, the Ordos basin, the Khondalite belt and the Yinshan terrane, as well as the entire Alxa block should be the focus of exploration.

Data from this study and previous studies (e.g., Li and Ripley, 2011) indicate that the Jinchuan intrusion is the product of rift-related (or mantle plume for some researchers) basaltic magmatism in a continental setting, temporally coinciding with the early stage of Rodinia breakup. This suggests that the potential of new discovery for another Jinchuan-type ore deposit still exists. In such a search, the first step is to find mafic-ultramafic intrusions with ages similar to that of the Jinchuan intrusion. The second step is to check if they have similar lithogeochemical characteristics, some of which are given above, to the Jinchuan intrusion. Geophysical exploration and drilling can then be used for those with similar lithological characteristics to the Jinchuan intrusion. The currently known mafic intrusion in the North China Craton with an age similar to that of the Jinchuan, i.e., the Luanchuan gabbroic intrusion (Fig. 1) is not a good exploration target because its lithogeochemical characteristics are significantly different from those of the Jinchuan intrusion.

7. Conclusions

New findings and important conclusions from this study are summarized below.

(1) The ~830 Ma Jinchuan Ni–Cu ore-bearing mafic-ultramafic intrusion in the Alxa block is the product of rift-related basaltic magmatism in a continental setting.
(2) Detrital zircon data support the model that the Alxa block and the adjacent Ordos block were amalgamated prior to the emplacement of the Jinchuan intrusion.
(3) The western parts of the North China Block have the best potential for new discoveries of Jinchuan-type Ni–Cu ore deposits.

Acknowledgments

This study was financially supported by the National Science Foundation of China (41072056, 40772058 and 41372095), the CAS/SAFEA International Partnership Program for Creative Research Teams (KZZD-EW-TZ-20), Key Laboratory of Western China's Mineral Resources of Gansu Province in Lanzhou University (WCRMGS-2014-04), China Geology Survey (12120114044401) and the State Key Laboratory of Ore Deposit Geochemistry of China (201110 and 201205). We thank Yulong Tian and Shuanjun Wu for their assistance in field work. The paper was written during Qingyan Tang's visit to Indiana University which was financially supported by the China Scholarship Council (201206180107).

Appendix A. Supplementary data

Supplementary data associated with this article can be found, in the online version, at http://dx.doi.org/10.1016/j.precamres.2014.08.015.

References

Charvet, J., 2013. The Neoproterozoic–Early Paleozoic tectonic evolution of the South China Block: an overview. J. Asian Earth Sci. 74, 198–209.
Dan, W., Li, X.-H., Guo, J., Liu, Y., Wang, X.-C., 2012a. Paleoproterozoic evolution of the eastern Alxa Block, westernmost North China: evidence from in situ zircon U–Pb dating and Hf–O isotopes. Gondwana Res. 21, 838–864.
Dan, W., Li, X.-H., Guo, J., Liu, Y., Wang, X.-C., 2012b. Integrated in situ zircon U–Pb age and Hf–O isotopes for the Helanshan khondalites in North China Craton: Juvenile crustal materials deposited in active or passive continental margin? Precambrian Res. 222–223, 143–158.
Darby, B.J., Gehrels, G.E., 2006. Detrital zircon reference for the North China block. J. Asian Earth Sci. 26, 637–648.
Gong, J.-H., Zhang, J.-X., Yu, S.-Y., 2011. The origin of Longshoushan Group and associated rocks in the southern part of the Alxa block: constraint from LA-ICP-MS U–Pb zircon dating. Acta Petrol. Mineral. 30, 795–818 (in Chinese with English abstract).
Gong, J.-H., Zhang, J.-X., Yu, S.-Y., 2013. Redefinition of the "Longshoushan Group" outcropped in the eastern segment of Longshoushan on the southern margin of Alxa Block: Evidence from detrital zircon U–Pb dating results. Acta Petrol. Mineral. 32, 1–22 (in Chinese with English abstract).
Hacker, B.R., Ratschbacher, L., Webb, L., Ireland, T., Walker, D., Dong, S., 1998. U/Pb zircon ages constrain the architecture of the ultrahigh-pressure Qinling–Dabie Orogen, China. Earth Planet. Sci. Lett. 161, 215–230.
Handley, H.K., Turner, S., Macpherson, C.G., Gertisser, R., Davidson, J.P., 2011. Hf–Nd isotope and trace element constraints on subduction inputs at island arcs: limitations of Hf anomalies as sediment input indicators. Earth Planet. Sci. Lett. 304, 212–223.
Hou, K.J., Li, Y.H., Tian, Y.Y., 2009. In situ U–Pb zircon dating using laser ablation-multi ion counting-ICP-MS. Miner. Deposits 28, 481–492 (in Chinese with English abstract).
Hu, J., Gong, W., Wu, S., Liu, Y., Liu, S., 2014. LA-ICP-MS zircon U-Pb dating of the Langshan Group in the Northeast margin of the Alax block, with tectonic implications. Precambrian Res., http://dx.doi.org/10.1016/j.precamres.2014.08.013.
Li, C., Ripley, E.M., 2011. The Giant Jinchuan Ni-Cu-(PGE) Deposit: tectonic setting, magma evolution, ore genesis and exploration implications. Rev. Econ. Geol. 17, 163–180.
Li, C., Ripley, E.M., Thakurta, J., Stifter, E.C., Qi, L., 2013. Variations of olivine Fo-Ni contents and highly chalcophile element abundances in arc ultramafic cumulates, southern Alaska. Chem. Geol. 351, 15–28.
Li, Q., Li, S., Zheng, Y.-F., Li., H., Massonnec, H.J., Wang, Q., 2003a. A high precision U–Pb age of metamorphic rutile in coesite-bearing eclogite from the Dabie Mountains in central China: a new constraint on the cooling history. Chem. Geol. 200, 255–265.
Li, X.H., Su, L., Chung, S.-L., Li, Z.X., Liu, Y., Song, B., Liu, D.Y., 2005. Formation of the Jinchuan ultramafic intrusion and the world's third largest Ni-Cu sulfide deposit: associated with the ~825 Ma south China mantle plume? Geochem. Geophys. Geosyst. 6, Q11004, http://dx.doi.org/10.1029/2005GC001006.
Li, Z.X., Li, X.H., Kinny, P.D., Wang, J., 1999. The breakup of Rodinia: did it start with a mantle plume beneath South China? Earth Planet. Sci. Lett. 173, 171–181.
Li, Z.-X., Li, X.-H., Zhou, H., Kinny, P.D., 2002. Grenvillian continental collision in south China: New SHRIMP U-Pb zircon results and implications for the configuration of Rodinia. Geology 30, 163–166.
Li, Z.X., Li, X.H., Kinny, P.D., Wang, J., Zhang, S., Zhou, H., 2003b. Geochronology of Neoproterozoic syn-rift magmatism in the Yangtze Craton South China and correlations with other continents: evidence for a mantle superplume that broke up Rodinia. Precambrian Res. 122, 85–109.
Lu, S., Zhao, G., Wang, H., Hao, G., 2008. Precambrian metamorphic basement and sedimentary cover of the North China Craton: a review. Precambrian Res. 160, 77–93.
Ludwig, K.R., 2003. User's manual for Isoplot 3.00: a geolocronolgical toolkit for Microsoft Excel, Berkeley. Berkeley Geochronological Center Special Publication, No. 4, 71 pp.
Pearce, J., 2008. Geochemical fingerprinting of oceanic basalts with applications to ophiolite classification and the search for Archean oceanic crust. Lithos 100, 14–48.
Peng, P., Guo, J.H., Zhai, M.G., Bleeker, W., 2010. Paleoproterozoic gabbronoritic and granitic magmatism in the northern margin of the North China Craton: evidence of crust–mantle interaction. Precambrian Res. 183, 635–659.
Peng, P., Wang, X., Windley, B.F., Guo, J., Zhai, M.G., Li, Y., 2014. Spatial distribution of ~1950–1800 Ma metamorphic events in the North China Craton: implications for tectonic subdivision of the craton. Lithos 202–203, 250–266.
Rudnick, R.L., Gao, S., 2003. Composition of the continental crust. In: Rudnick, R.L. (Ed.), Treatise on Geochemistry, v. The Crust. Elsevier, Amsterdam, pp. 1–64.
Salters, V.J.M., Mallick, S., Hart, S.R., Langmuir, C.E., Stracke, A., 2011. Domains of depleted mantle: new evidence from hafnium and neodymium isotopes. Geochem. Geophys. Geosyst. 12, Q08001, http://dx.doi.org/10.1029/2011GC003617.
Santosh, M., 2010. Assembling North China Craton within the Columbia supercontinent: the role of double-sided subduction. Precambrian Res. 178, 149–167.
Song, S., Niu, Y., Su, L., Xia, X., 2013. Tectonics of the North Qilian orogen, NW China. Gondwana Res. 23, 1378–1401.
Tung, K.A., Yang, H.Y., Liu, D.Y., Zhang, J.X., Tseng, C.Y., Wan, Y.S., 2007. SHRIMP U–Pb geochronology of the detrital zircons from the Longshoushan Group and its tectonic significance. Chin. Sci. Bull. 52, 1414–1425.
Wang, X.-L., Jiang, S.-Y., Dai, B.-Z., Griffin, W.L., Dai, M.-N., Yang, Y.-H., 2011. Age, geochemistry and tectonic setting of the Neoproterozoic (ca 830 Ma) gabbros on the southern margin of the North China Craton. Precambrian Res. 190, 35–47.
Williams, I.S., 1998. U-Th-Pb geochronology by ion microprobe. Rev. Econ. Geol. 7, 1–35.
Wood, B.J., Blundy, J.D., 2003. Trace element partitioning under crustal and uppermost mantle conditions: the influences of ionic radius, cation charge, pressure and temperature. In: Carlson, R.W. (Ed.), The Mantle and Core. Treatise on Geochemistry, vol. 2. Elsevier, Amsterdam, pp. 395–424.
Wu, F.-Y., Yang, Y.-H., Xie, L.-W., Yang, J.-H., Xu, P., 2006. Hf isotopic compositions of the standard zircons and baddeleyites used in U–Pb geochronology. Chem. Geol. 234, 105–126.
Xiao, W., Windley, B.F., Hao, J., Zhai, M., 2003. Accretion leading to collision and the Permian Solonker suture, Inner Mongolia, China: Termination of the central Asian orogenic belt. Tectonics 22, 1069, doi:10.1029/2002TC001484, 6.
Yogodzinski, G.M., Vervoort, J.D., Brown, S.T., Gerseny, M., 2010. Subduction controls of Hf and Nd isotopes in lavas of the Aleutian island arc. Earth Planet. Sci. Lett. 300, 226–238.
Yu, J.-H., O'Reilly, S.Y., Wang, L., Griffin, W.L., Zhou, M.-F., Zhang, M., Shu, L., 2010. Components and episodic growth of Precambrian crust in the Cathaysia Block South China: evidence from U–Pb ages and Hf isotopes of zircons in Neoproterozoic sediments. Precambrian Res. 181, 97–114.
Yuan, W., Yang, Z., 2014. The Alashan Terrane was not part of North China by the Late Devonian: evidence from detrital zircon U–Pb geochronology and Hf isotopes. Gondwana Res., http://dx.doi.org/10.1016/j.gr.2013.12.009.
Zhai, M.-G., Santosh, M., 2011. The early Precambrian odyssey of North China Craton: a synoptic overview. Gondwana Res. 20, 6–25.
Zhang, J., Gong, J., Yu, S., Li, H., Hou, K., 2013. Neoarchean–Paleoproterozoic multiple tectonothermal events in the western Alxa block North China Craton and their geological implication: evidence from zircon U–Pb ages and Hf isotopic composition. Precambrian Res. 235, 36–57.
Zhang, J., Li, J., Liu, J., Feng, Q., 2011. Detrital zircon U–Pb ages of Middle Ordovician flysch sandstones in the western Ordos margin: new constraints on their provenances, and tectonic implications. J. Asian Earth Sci. 42, 1030–1047.
Zhang, J., Li, J.Y., Liu, J.F., Qu, J.F., Feng, Q.W., 2012. The relationship between the Alxa Block and the North China Plate during the Early Paleozoic: new information from the Middle Ordovician detrital zircon ages in the eastern Alxa Block. Acta Petrol. Sin. 28, 2912–2934 (in Chinese with English abstract).
Zhang, M., Kamo, S.L., Li, C., Hu, P., Ripley, E.M., 2010. Precise U-Pb zircon-baddeleyite age of the Jinchuan sulfide ore-bearing ultramafic intrusion, western China. Mineral. Deposita 45, 3–9.

Zhang, M., Tang, Q., Hu, P., Ye, X., Cong, Y., 2013. Noble gas isotopic constraints on the origin and evolution of the Jinchuan Ni–Cu–(PGE) sulfide ore-bearing ultramafic intrusion, Western China. Chem. Geol. 339, 301–312.

Zhao, G., Cawood, P.A., 1999. Tectonothermal evolution of the Mayuan Assemblage in the Cathaysia Block: implications for Neoproterozoic collision-related assembly of the South China Craton. Am. J. Sci. 299, 309–339.

Zhao, G., Cawood, P.A., 2012. Precambrian geology of China. Precambrian Res. 222–223, 13–54.

Zhao, G., Wilde, S.A., Cawood, P.A., Sun, M., 2001. Archean blocks and their boundaries in the North China Craton: lithological, geochemical, structural and P–T path constrains and tectonic evolution. Precambrian Res. 107, 45–73.

Zhao, G., Sun, M., Wilde, S.A., Li, S., 2005. Late Archean to Paleoproterozoic evolution of the North China Craton: key issues revisited. Precambrian Res. 136, 177–202.

Zhao, G., Wilde, S.A., Sun, M., Guo, J., Kröner, A., Li, S., Li, X., Wu, C., 2008. SHRIMP U–Pb zircon geochronology of the Huaian Complex: constraints on Late Archean to Paleoproterozoic crustal accretion and collision of the Trans-North China Orogen. Am. J. Sci. 308, 270–303.

Zhao, G., Wilde, S.A., Guo, J., Cawood, P.A., Sun, M., Li, X., 2010. Single zircon grains record two Paleoproterozoic collisional events in the North China Craton. Precambrian Res. 177, 266–276.